Supporting Information for:

Elucidating Gas-Surface Interactions Relevant to Atmospheric Particle Growth using Combined Temperature Programmed Desorption and Temperature-Dependent Uptake

Kristen N. Johnson, Yixin Li,[a] Michael J. Ezell, Pascale S. J. Lakey, Manabu Shiraiwa and Barbara J. Finlayson-Pitts

Department of Chemistry, University of California, Irvine, Irvine, CA 92697-2025

[a]Now at: Department of Atmospheric Sciences, Texas A&M University, College Station, TX 77843

Correspondence: Barbara J. Finlayson-Pitts (bjfinlay@uci.edu)

Contents **Page**

Detailed Description of the Apparatus

The main chamber consists of a stainless steel six way cross sealed by 6 in flanges. For reference, flanges that vacuum seal the cross are designated by the points of the compass (north, south, east, west) plus top and bottom. The measured chamber volume is 5260 cm^3 and the estimated interior surface area is 2360 cm^2. The majority of stainless-steel parts and vacuum feedthroughs were obtained from Kurt J. Lesker Company (KJLC). Unless noted otherwise, all flanges are of the ConFlat UHV type and are sealed by compressed copper gaskets. Also, unless noted otherwise, machining for flanges and specialized parts was performed in house at the UCI machine shop, and all welds were formed from the vacuum side of flanges.

Bottom Flange: Sample Stage and Temperature Control. The bottom flange holds the removable sample cup and separates the cross from the cryogenic/heating parts of the apparatus. Temperature control of the sample is provided by balancing heating and cooling of a copper stub and rod in contact with the indium and the bottom of the sample cup. The sample cup sits inside a well whose bottom disc is brazed to the bottom rim of a thin walled (0.008 in) stainless steel cylinder. which is brazed at the top to a 6 in flange that is sealed to the six-way cross. This forms a pocket into which a removable sample cup fits for facile sample preparation and removal (Fig. S1). Temperature-control of the sample cup is provided from 100 K to 400 K. The lower end of the temperature range is limited by the heat transfer between the sample holder and the thin-walled stainless steel cylinder. The upper end of the temperature range is limited by the melting temperature of the indium foil. A thermocouple mounted in the center of the terminal stage is used to monitor the temperature during experiments. The temperature measured here agrees within ±1 K of that measured with a thermocouple mounted in the base of the sample cup (Table S1).

The temperature of the fixed sample stage and thus the bottom of the sample cup is controlled by cooling the lowest part of the copper rod assembly using liquid nitrogen and simultaneously heating by applying a current to a nichrome wire wound around the copper rod. Electrical power to the heating wire is supplied by a Eurotherm EFit power supply connected to a Eurotherm 3216 temperature controller. This is connected via an EIA 485 communications converter to a computer with iTools software v9 for data acquisition and monitoring. Temperature programming in the range of 100 K to 400 K is possible at a constant rate of up to 0.5 K s^{-1}. This upper heating rate is limited by the current limit of the temperature controller which was set to 10 A for safety reasons. The temperature of a thermocouple mounted in the center of the fixed copper stub is within ± 1 K of that measured with a thermocouple mounted in the base of the sample cup in separate experiments (Table S1).

Removable Sample Cup. The removable sample cup (Fig. S1) consists of a copper disc that is gold-coated for inertness and attached to a thin-walled PEEK cylinder to minimize heat transfer from the bottom disc to the walls of the cup. The samples are placed on the bottom of the removable sample cup, so they are in thermal contact with the temperature-controlled sample stage. A second PEEK cylinder fits snugly inside the removable sample cup and can be pressed down with a threaded Teflon ring for improved thermal contact. Samples of potential interest include solids, e.g. powders, or flat surfaces such as silicon wafers that have been treated in different ways (e.g. derivatized with self-assembled monolayers) to present a well-defined surface composition to the incoming gas.

Top Flange. The top flange of the main chamber holds a linear feedthrough (Fig. 1a). For uptake measurements, a stainless-steel disc is attached to the linear feedthrough and serves as a cover for the sample holder. Alternatively, for TPD measurements, a gas doser is attached to the

linear feedthrough to introduce gases for even deposition of the gas across the sample surface (Fig. S2).

North, South, East, and West Flanges. The north flange (Fig. S3) serves as a mount for a magnetically driven rotatable feedthrough that allows for the selection of orifices of different diameters (0.5, 1, 2, 4, 8, 11 and 14 mm) that are machined around the periphery of a stainless-steel disk. The orificies are rotated in front of a fixed opening (17 mm) in a Teflon disk that leads to a quadrupole mass spectrometer (QMS, Extrel Core Mass Spectrometer) equipped with an electron impact ionization source. The south flange has a hinged easy access viewport to insert or remove the sample cup. It also provides a line-of-sight to view the selected orifice and ensure it is centered over the opening to the mass spectrometer. The west flange, located in the horizontal direction, has three 0.25 in stainless steel tubes welded to the flange to provide gas inlets. The east flange has two half nipples welded off center that connect to an ionization gauge and a pressure gauge to measure the pressure in the main cell during pump-down and in the presence of the flow of the reactant gases.

Due to limitations on the pumping speed from the tubing conductance connecting the north flange to the QMS, the effective orifice diameter is somewhat different from the nominal value. To account for this, the effective orifice diameters, $D_{\text{eff.}}$, were calibrated using experimental measurements of the escape rate of selected gases. These are summarized in Table S2.

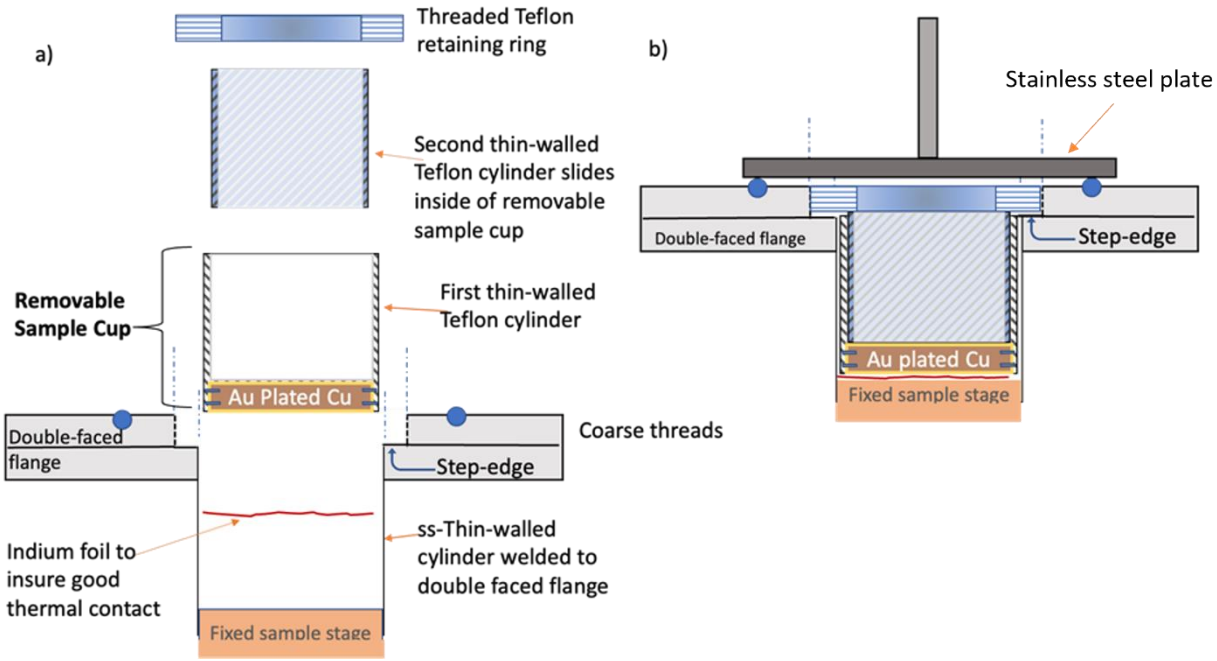

Figure S1 a) Expanded view of the removable sample cup with associated parts; and b) assembled view with stainless-steel plate at the end of the linear feedthrough that rests on an o-ring to separate the sample from the main body of the 6-way cross.

Table S1. Temperatures (K) and temperature difference between the thermocouple mounted in the sample stage and that in the sample cup.

T_{stage}	T_{cup}	dT
298.7	297.9	0.8
293.1	291.9	1.3
288.1	287.0	1.1
282.7	281.5	1.2
278.1	277.4	0.7
272.9	272.7	0.2
268.0	268.3	-0.3
263.1	263.6	-0.5
257.1	257.8	-0.7
251.9	252.7	-0.8
242.4	243.1	-0.7
237.8	238.5	-0.7
232.2	232.9	-0.7
225.7	226.4	-0.7
223.0	224.0	-1.0
213.1	214.5	-1.4
201.1	202.2	-1.1
193.2	194.3	-1.1
183.0	184.1	-1.1
173.0	173.8	-0.8
162.7	163.3	-0.6
153.0	153.4	-0.4
143.2	143.0	0.2
133.1	132.4	0.7
128.1	127.1	1.0
123.1	121.6	1.5
118.1	117.1	1.0
113.1	112.1	1.0
105.2	105	0.2

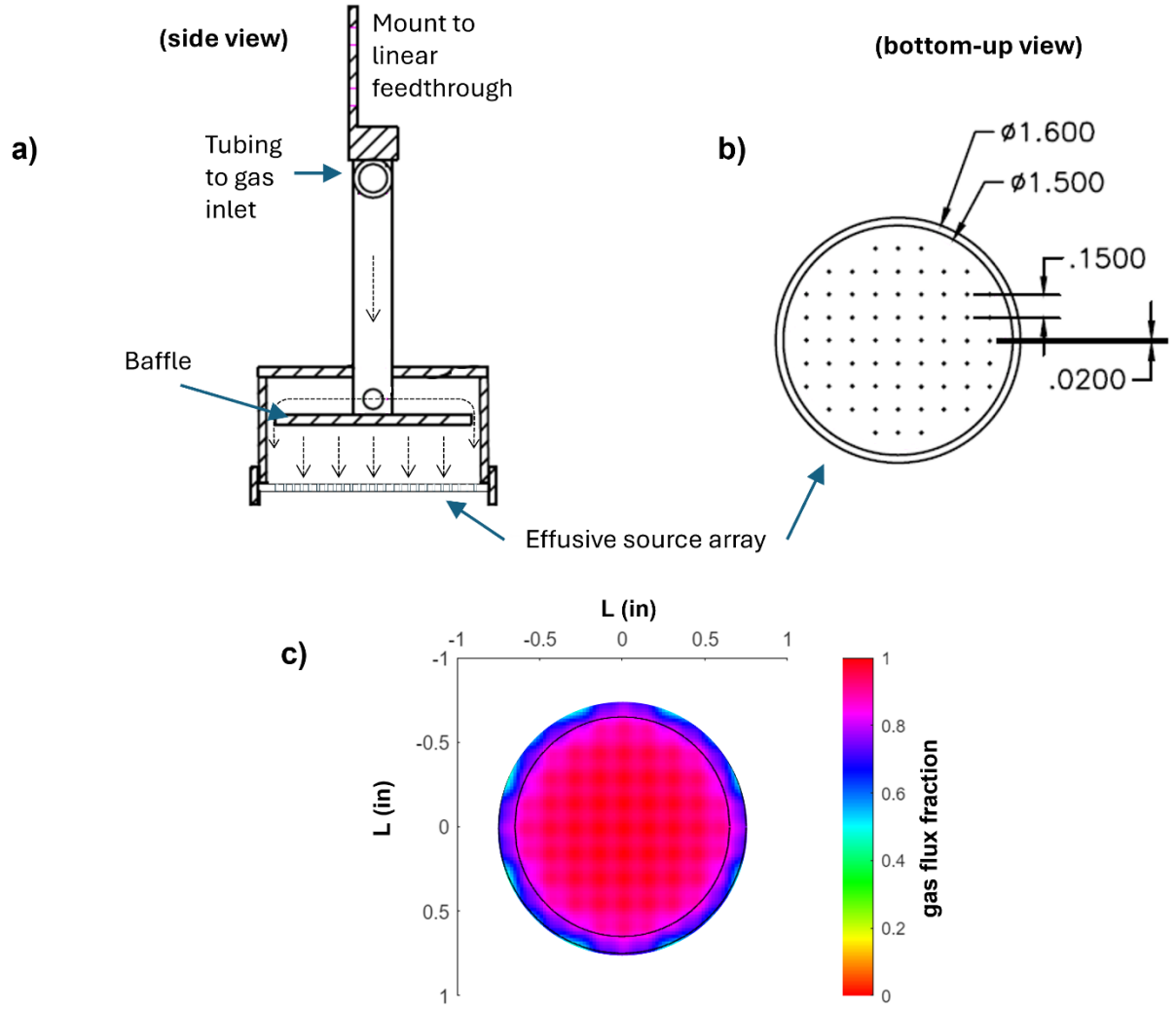

Figure S2. Schematic of the gas doser which uses an array of effusive orifices to deliver gases in a uniform manner across the sample surface, a) side view, b) bottom-up view of orifice placement, dimensions are in inches. Dashed arrows in a) denote the direction of the flow of gases. The thickness of the effusive orifice plate is 0.005 in. c) Gas flux fraction across the array of orifices. This design gives a flux gradient with 85% or better uniformity across an area marked with the black circle which has an area of 1.32 in^2. This is calculated from assuming a flux per unit area of the sample $G(\sigma) = \cos^4(\sigma)/\pi$ where σ is the angle to the source axis and the distance between the doser and the sample is 0.15 in.[1]

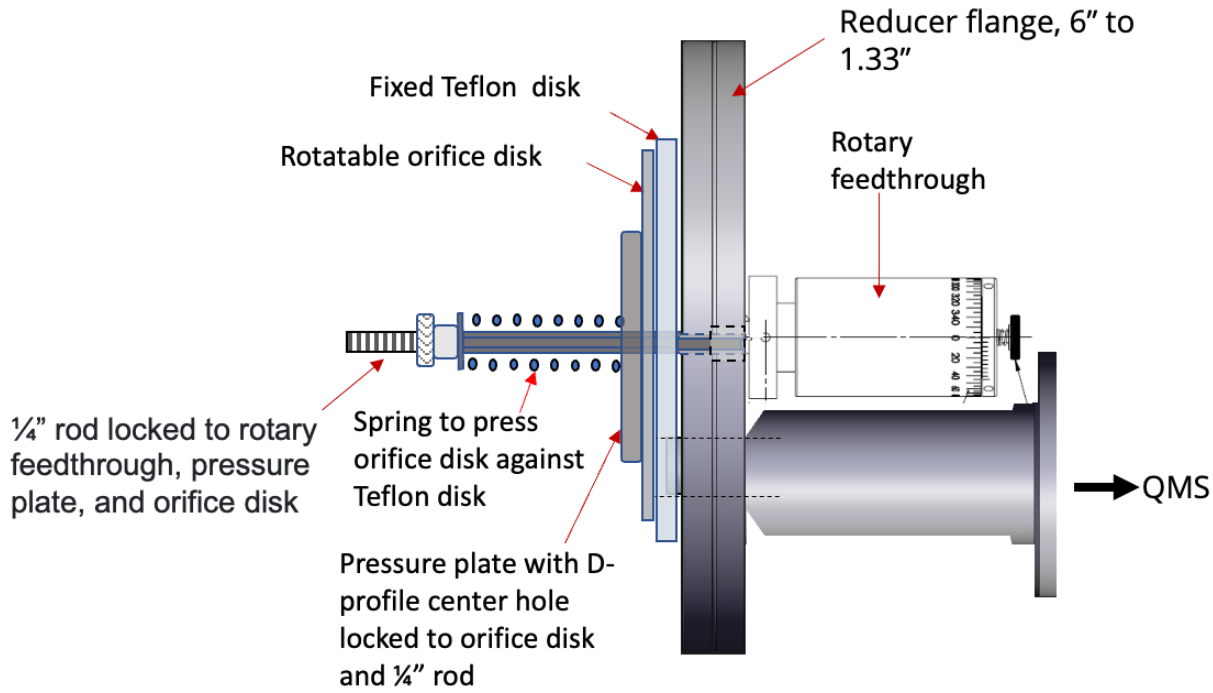

Figure S3. North Flange and components. Tension on the spring is adjusted to hold the rotatable orifice disk snugly against the fixed Teflon disk. QMS = quadrupole mass spectrometer.

Table S2. Gas escape rates and effective orifice diameters at 298 K.[a]

$D_{geometric}$ (mm)	$k_{esc,\ benzene}$ (s^{-1})	$k_{esc,\ methanol}$ (s^{-1})	$k_{esc,\ chloropentane}$ (s^{-1})	$k'=k_{esc}\cdot M^{0.5}$ ($s^{-1}(g\ mol^{-1})^{0.5}$) [b]	$D_{eff.}$ (mm) [c]
14	0.560	0.700	0.462	4.90 ± 0.23	7.2 ± 0.2
11	0.450	0.577	0.370	4.01 ± 0.21	6.6 ± 0.2
8	0.360	0.398	0.277	3.12 ± 0.10	5.8 ± 0.2
4	0.125	0.112	0.098	0.96 ± 0.23	3.2 ± 0.4
2	0.037	0.037	0.028	0.30 ± 0.06	1.8 ± 0.2
1	0.011	0.012	0.009	0.09 ± 0.02	1.0 ± 0.1
0.5	0.007	0.007	0.005	0.05 ± 0.01	0.7 ± 0.1

[a] From the measurement of signal decay for benzene, 1-chloropentane, and methanol at 298K, uncertainty is 1σ.

[b] M = molar mass of gas molecule in units of g $mole^{-1}$, and k' is independent of mass.

[c] Explanation of D_{eff}.

Defining $k_{esc} = ZA_{orifice,\ effective} = Z\pi(D_{eff.}/2)^2$, where A is the area of the orifice and Z is the gas-chamber wall collision rate and is equal to: $Z = \left(\frac{1}{4V}\right)\sqrt{\frac{8RT}{\pi M}}$ where V is the chamber volume (5260 cm^3), from there rearranging gives: $D_{eff.} = 2\sqrt{\frac{k_{esc}}{\pi Z}}$

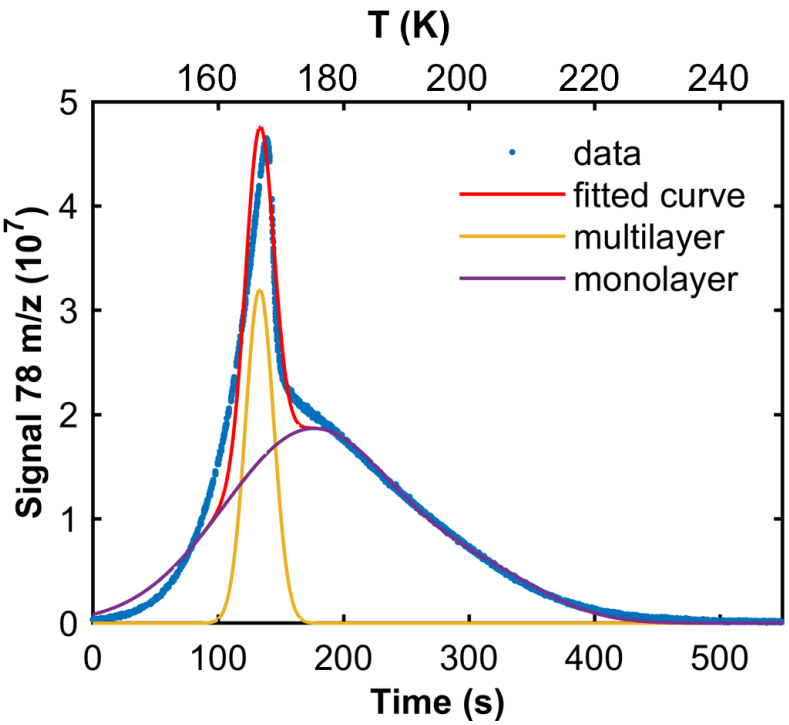

Figure S4. Example of the deconvolution of the multilayer and the monolayer desorption peaks for benzene from Cabosil. The narrow yellow curve corresponds to the multilayer desorption for benzene desorbing from a layer of benzene at 162 K. The broad curve corresponds to monolayer desorption, benzene desorbing from the silicon oxide surface. The area under the monolayer curve was used to determine the accessible surface area in all experiments based on the calibrated mass spectrometer signal and the cross-sectional area of each molecule. The temperature ramp rate was 0.2 K/s.

Kinetic Model Description

Figure S5 shows a schematic of the multilayer kinetic model used in this work. The model uses a flux-based approach to describe vertical diffusion through the pores between silica particles and reversible adsorption of compounds to the silica particle surfaces. Concentrations in the chamber gas phase, $[X]_g$ (molecules cm^{-3}), in the first pore layer, $[X]_{p,1}$, (molecules cm^{-3}), in the middle pore layers, $[X]_{p,j}$, (molecules cm^{-3}), in the last pore layer , $[X]_{p,n}$, (molecules cm^{-3}), and adsorbed to the silica in each layer, $[X]_{ads,j}$, (molecules cm^{-2}), are calculated as a function of time by solving a series of differential equations as shown below:

$$\frac{d[X]_g}{dt} = k_{in}[X]_{g,0} - k_{out}[X]_g + (J_{diff,p1,g} - J_{diff,g,p1})\frac{F_{pores}A_{sil}}{V} \quad \text{(E1)}$$

$$\frac{d[X]_{p,1}}{dt} = (J_{diff,g,p1} - J_{diff,p1,g})\frac{1}{\delta_{layer}} + (J_{diff,p2,p1} - J_{diff,p1,p2})\frac{1}{\delta_{layer}} + (J_{des,1} - J_{ads,1})\frac{S_{sil}}{A_{sil}\delta_{sil}F_{pores}} \quad \text{(E2)}$$

$$\frac{d[X]_{p,j}}{dt} = (J_{diff,pj-1,pj} - J_{diff,pj,pj-1})\frac{1}{\delta_{layer}} + (J_{diff,pj+1,pj} - J_{diff,pj,pj+1})\frac{1}{\delta_{layer}} + (J_{des,j} - J_{ads,j})\frac{S_{sil}}{A_{sil}\delta_{sil}F_{pores}} \quad \text{(E3)}$$

$$\frac{d[X]_{p,n}}{dt} = (J_{diff,pn-1,pn} - J_{diff,pn,pn-1})\frac{1}{\delta_{layer}} + (J_{des,n} - J_{ads,n})\frac{S_{sil}}{A_{sil}\delta_{sil}F_{pores}} \quad \text{(E4)}$$

$$\frac{d[X]_{ads,j}}{dt} = J_{ads,j} - J_{des,j} \quad \text{(E5)}$$

where k_{in} (s^{-1}) and k_{out} (s^{-1}) are the first-order rates of molecules entering the chamber and being removed from the chamber, respectively. $[X]_{g,0}$ (molecules cm^{-3}) is the gas-phase concentration flowing into the chamber, F_{pores} is the volume fraction of pores in the deposited silica, A_{sil} (cm^2) is the geometric surface area of the spot that the particles form, V (cm^3) is the volume of the chamber, δ_{layer} (cm) is the thickness of a layer in the model, S_{sil} (cm^2) is the total surface area of the silica particles and δ_{sil} (cm) is the total thickness of the silica particles. $J_{ads,j}$ (cm^{-2} s^{-1}) and $J_{des,j}$ (cm^{-2} s^{-1}) are the adsorption and desorption fluxes to and from the silica surface in layer j, respectively. $J_{diff,g,p1}$ (cm^{-2} s^{-1}) and $J_{diff,p1,g}$ (cm^{-2} s^{-1}) are the diffusion fluxes from the gas phase to the first layer of pores and from the first layer of pores to the gas phase, respectively. $J_{diff,pj,pj+1}$ (cm^{-2} s^{-1}) and $J_{diff,pj,pj-1}$ (cm^{-2} s^{-1}) are the diffusion fluxes from layer j to layers j+1 and j-1, respectively.

Adsorption and desorption fluxes in the model are based on equations from the kinetic double-layer model of aerosol surface chemistry and gas-particle interactions (K2-SURF)[2] and are consistent with Langmuir's theory of adsorption. Diffusion in the pores between the particles is assumed to follow Fick's first law of diffusion. For simplicity, the same diffusion coefficient is assumed between each layer in the model and the total silica particle surface area is split evenly between the model layers. The number of model layers (n) has been increased until convergence in the results is obtained. A list of parameters used in the model are presented in Table S2 alongside explanations of the values. The desorption rate of molecules from the silica surface and the diffusion coefficient through the gas-phase pores were the only unknown parameters and were varied until the model could replicate the experimental measurements. Note that the pressure was reset in the model each time the lid was closed, but drifting signals or pressures that occurred while the lid was open have not been treated.

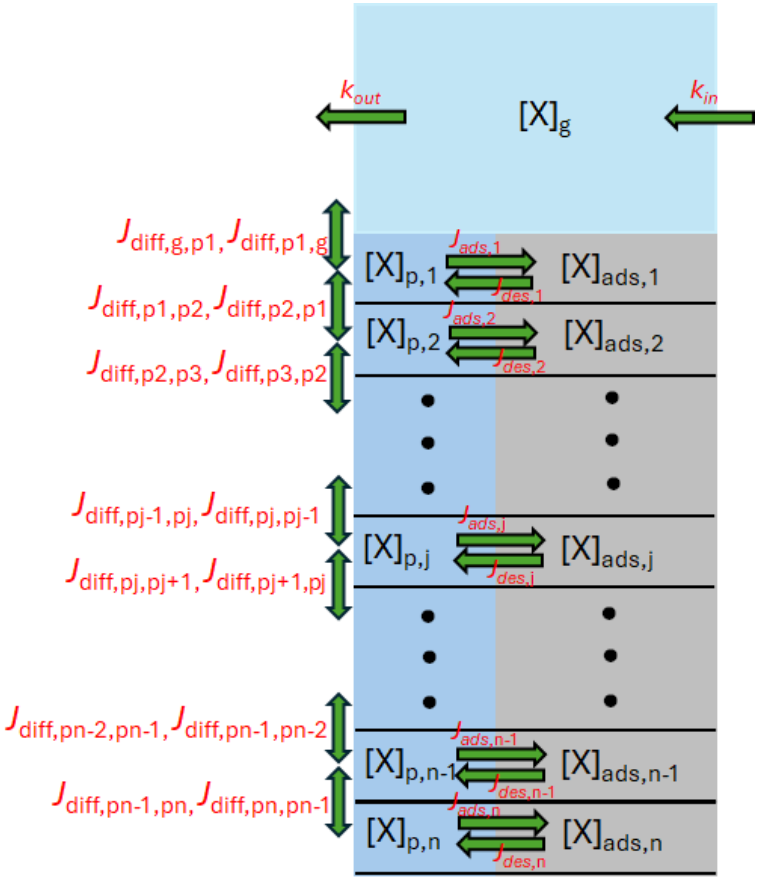

Figure S5: A schematic of the multilayer kinetic model.

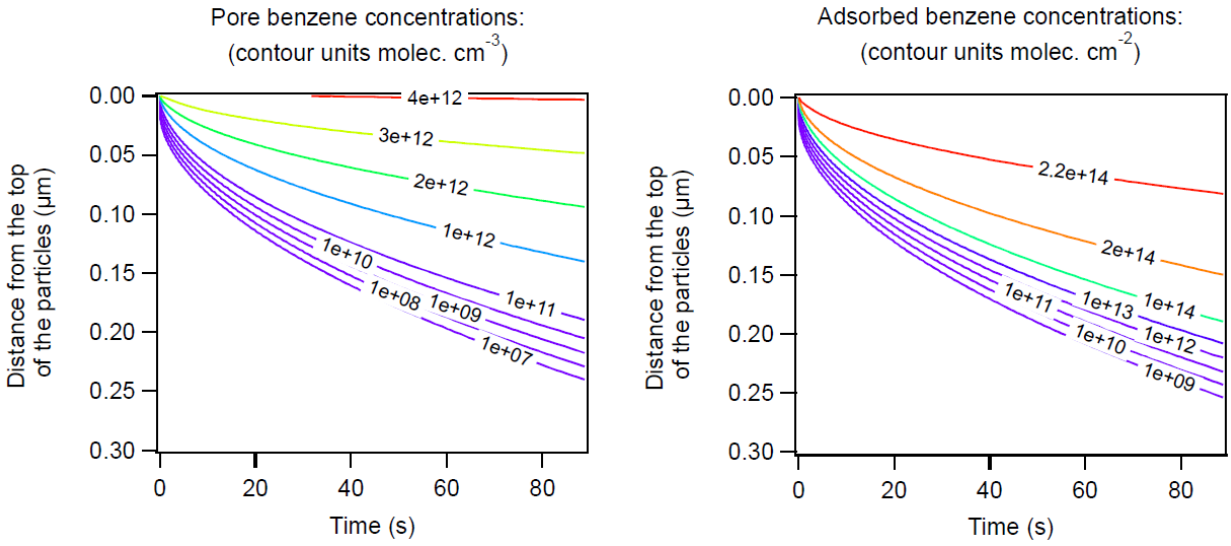

Figure S6. Results of multilayer model simulations for initial benzene concentration 7.3×10^{-5} Torr (4.2×10^{12} molecules cm^{-3}). Showing gas phase benzene concentrations in the pores (left) and surface concentrations adsorbed on the silica particles (right) as a function of depth within the bed of particles.

Table S3. Parameters used in the kinetic model.

Parameter	Description	Parameter values			Additional information
		Benzene	**Methanol**	**Chloropentane**	
k_{out}	First order removal rate of molecules from the chamber.	0.589 s^{-1}	0.7 s^{-1}	0.46 s^{-1}	Experimental value (k_{esc})
k_{in}	First order rate of molecules entering the chamber.	0.589 s^{-1}	0.7 s^{-1}	0.46 s^{-1}	Same as k_{out}
T	Temperature	170 K	170 K	170 K	Experimental value
σ	Surface area of 1 molecule	4.3×10^{-15} cm^2	2.1×10^{-15} cm^2	4.0×10^{-15} cm^2	Literature value[3]
A_{sil}	Geometric surface area of the spot that the particles form.	3.14 cm^2	7.85 cm^2	7.85 cm^2	Experimental value based on mass of particles used
S_{sil}	Total surface area of the silica particles	2000 cm^2	5000 cm^2	5000 cm^2	Experimental value (determined from N_2 adsorption) based on mass of particles used
V	Volume of the chamber	5260 cm^3	5260 cm^3	5260 cm^3	Experimental value
δ_{sil}	Thickness of the deposited particles	1.77 μm	1.77 μm	1.77 μm	A hexagonal closed packed packing structure is assumed.
F_{sil}	Volume fraction of silica in the layers of deposited silica particles.	0.74	0.74	0.74	
F_{pores}	Volume fraction of gas (or pores) in the layers of deposited silica particles.	0.26	0.26	0.26	
$\alpha_{s,0}$	Surface accommodation coefficient on an adsorbate free silica surface	1	1	1	Typical value
k_d	Desorption rate coefficient of molecules from the silica surface.	3 s^{-1}	0.4 s^{-1}	0.1 s^{-1}	Fitting value
D_p	Diffusion coefficient through the gas-phase pores.	0.001 cm^2 s^{-1}	0.0012 cm^2 s^{-1}	0.0015 cm^2 s^{-1}	Fitting value

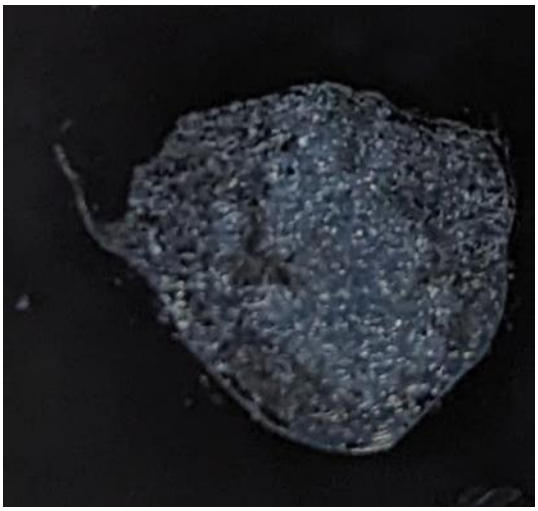

Figure S7. Top-down view photo of 1 mg of Cabosil deposited from an aqueous 10 mg/ml suspension onto an Ar plasma cleaned silicon wafer. Particles form a cylindrical bed with approximately 2 cm diameter and 2 μm depth assuming uniform hexagonal close packing of 100 nm particles.

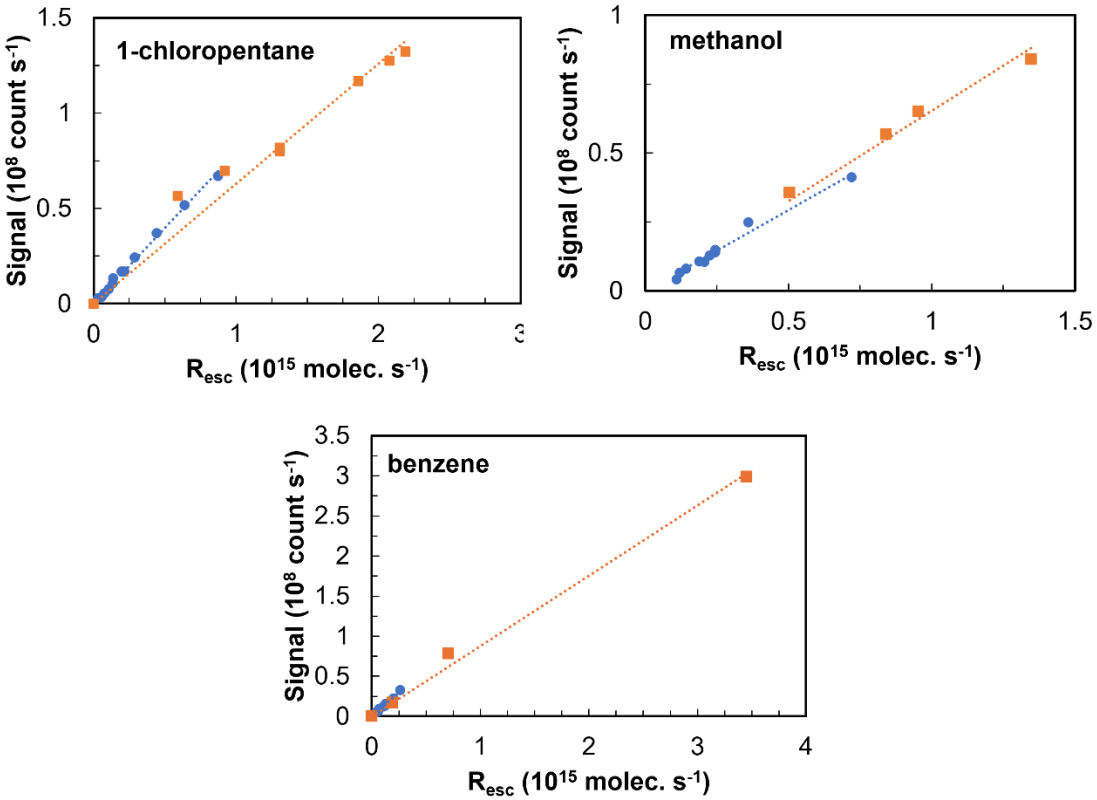

Figure S8. Calibration curves used for the uptake experiments for all adsorbates. The data for the 2 mm (blue circles) and for the 14 mm (orange squares) orifices are shown. Linear regression lines of best fit (dotted lines) are also shown. The rate of escape in molecules s^{-1} is calculated by $R_{esc} = k_{esc}\ N$ where k_{esc} is experimentally measured (Table S2) from the signal decay and N is number of molecules in the chamber calculated from the chamber pressure using the ideal gas law.

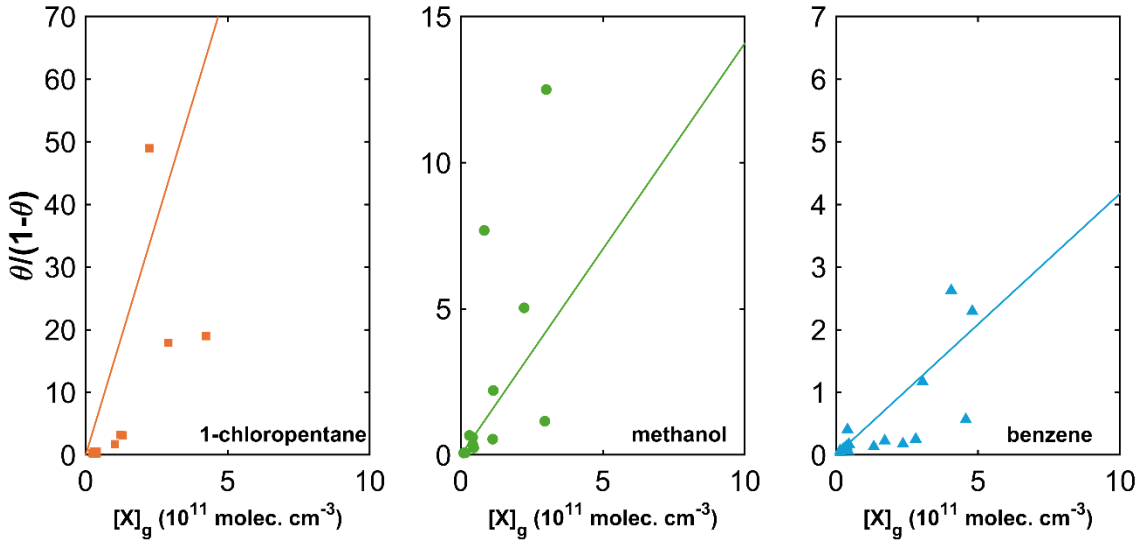

Fig. S9. Langmuir isotherm and line of best fit for 1-chloropentane, methanol, and benzene. The slope of the linear curve plotted here is equal to K and this fitted value was used in Eq. 2 to plot the solid curve in Fig. 4.

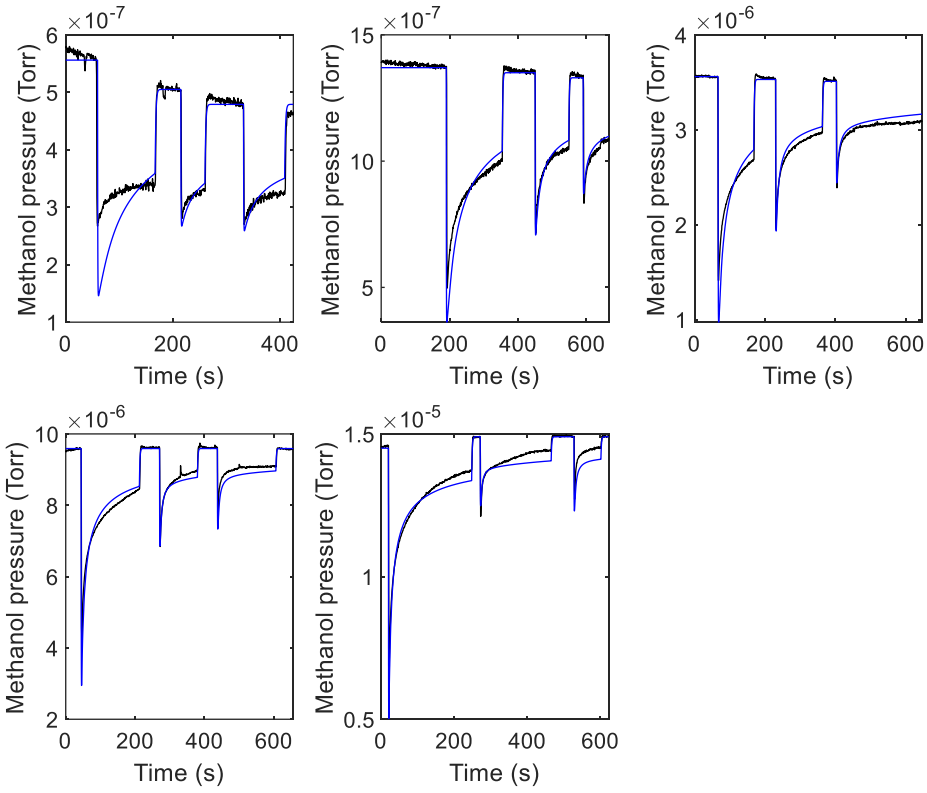

Figure S10: Measurements (black) and kinetic model results (blue) for the uptake of methanol onto silica particles for different initial methanol pressures.

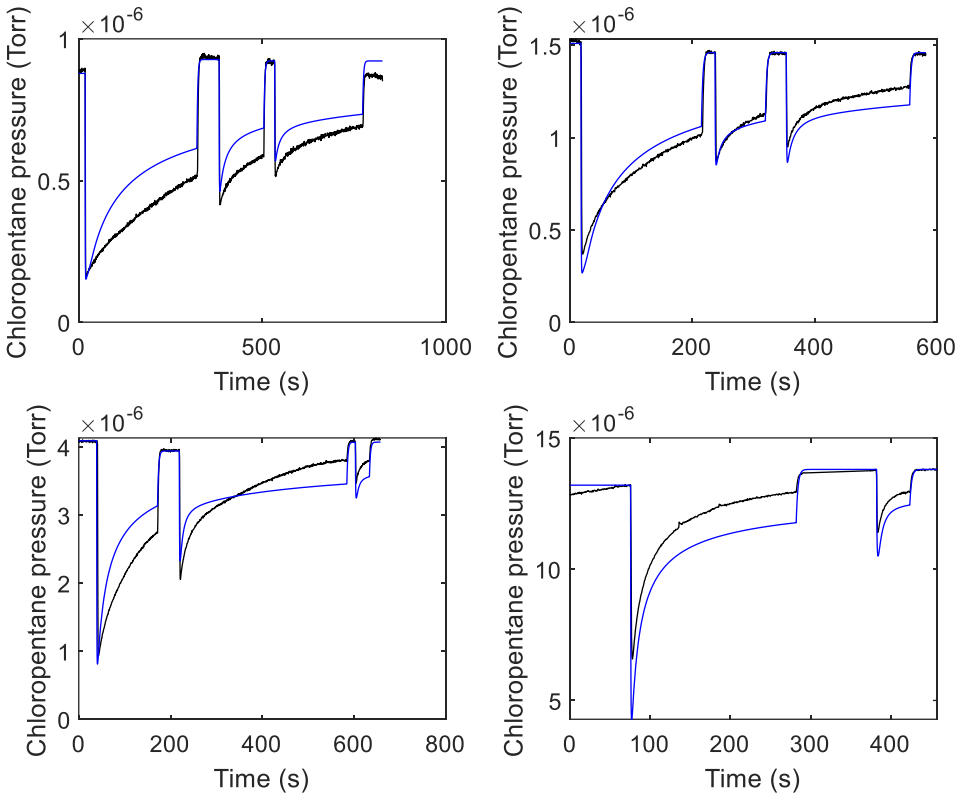

Figure S11: Measurements (black) and kinetic model (blue) results for the uptake of chloropentane onto silica particles for different initial chloropentane pressures.

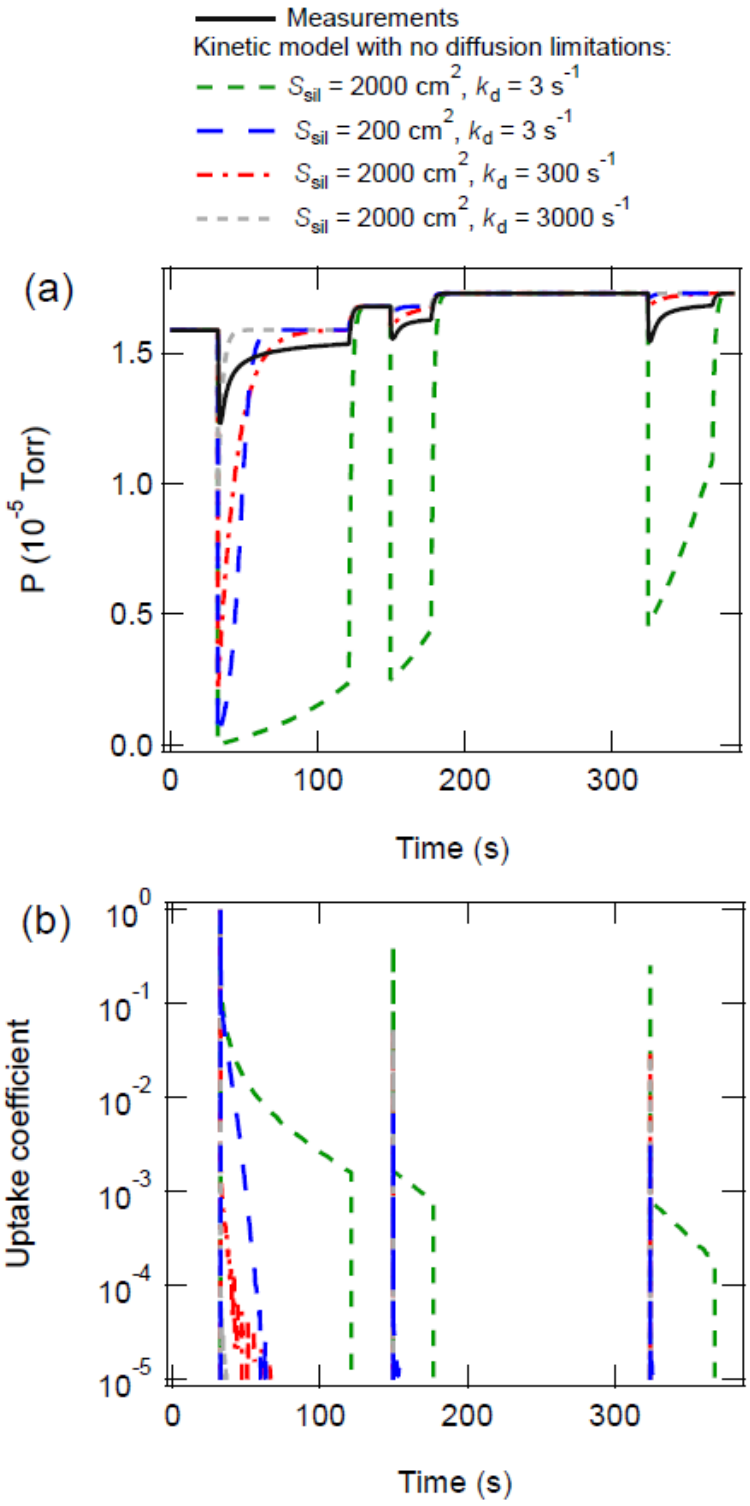

Figure S12: Model results for (a) benzene uptake to silica particles in the absence of diffusion limitations and (b) the corresponding uptake coefficients.

References

1. Kuhl, D. E.; Tobin, R. G., On the Design of Capillary and Effusive Gas Dosers for Surface Science. *Review of Scientific Instruments* **1995**, *66*, 3016-3020.
2. M. Shiraiwa, R. M. Garland and U. Pöschl, Kinetic double-layer model of aerosol surface chemistry and gas-particle interactions (K2-SURF): Degradation of polycyclic aromatic hydrocarbons exposed to O_3, NO_2, H_2O, OH and NO_3, *Atmos. Chem. Phys.*, 2009, **9**, 9571-9586.
3. Sing, K. S. W. 7 - Assessment of Surface Area by Gas Adsorption. In *Adsorption by Powders and Porous Solids (Second Edition)*; Rouquerol, F., Rouquerol, J., Sing, K. S. W., Llewellyn, P., Maurin, G., Eds.; Academic Press: Oxford, 2014; pp 237–268.